Universal dynamics of biological pattern formation in spatio-temporal morphogen variations

Mohit P. Dalwadi[1, 2, *] and Philip Pearce[1, 2, †]

[1] *Department of Mathematics, University College London*
[2] *Institute for the Physics of Living Systems, University College London*

Abstract. In biological systems, chemical signals termed morphogens self-organise into patterns that are vital for many physiological processes. As observed by Turing in 1952, these patterns are in a state of continual development, and are usually transitioning from one pattern into another. How do cells robustly decode these spatio-temporal patterns into signals in the presence of confounding effects caused by unpredictable or heterogeneous environments? Here, we answer this question by developing a general theory of pattern formation in spatio-temporal variations of "pre-pattern" morphogens, which determine gene-regulatory network parameters. Through mathematical analysis, we identify universal dynamical regimes that apply to wide classes of biological systems. We apply our theory to two paradigmatic pattern-forming systems, and predict that they are robust with respect to non-physiological morphogen variations. More broadly, our theoretical framework provides a general approach to classify the emergent dynamics of pattern-forming systems based on how the bifurcations in their governing equations are traversed.

Introduction. In biological pattern formation, cells interpret morphogen signals to make developmental decisions based on their location in a tissue, organ, embryo or population. Such systems have been found to be remarkably robust to a wide range of sources of variation between different cells or tissues in morphogen signals and system components [1, 2]. For example, in recent work, general principles of biological pattern-forming systems have been identified that promote robustness with respect to variations in morphogen and protein production rates [1, 3], in tissue or organism size [4, 5], and in gene-regulatory network architecture [6]. However, less is understood about how such systems respond to spatio-temporal variations in morphogen concentrations within individual cells, populations or tissues, particularly over timescales faster than or similar to growth.

Recent experimental and theoretical work has demonstrated how specific gene-regulatory network architectures convert spatio-temporal morphogen signals into a required static or dynamic response [7–12]. This morphogen "pre-pattern" can arise as a necessary part of the developmental process [7, 13, 14]. However, unpredictable morphogen fluctuations in a system may be caused by intrinsic noise [15], growth [16], cell motility or rearrangement [17–20], biochemical reactions [21, 22], or external flows [11, 23–25]. These studies raise the question of how to quantify the robustness of a system's gene-regulatory network output, i.e. emergent spatio-temporal patterning, with respect to variations in its pre-pattern morphogen input over a certain timescale.

Analysis of Canonical Equations. Reaction-diffusion systems, which are thought to underlie various mechanisms of biological pattern formation [7], self-organise in space and time via bifurcations in their governing equations [26]. Dynamics are typically observed to slow down near bifurcations [27] (see Supplemental Material), but the implications of this in the context of biological pattern formation are not understood. As a reaction-diffusion system undergoes a bifurcation, its dynamics can typically be approximated by a (low-dimensional) canonical weakly nonlinear equation whose form depends on the type of bifurcation [27]. Under such an approximation, the effects of spatio-temporal variations in system parameters are captured by corresponding variations in the parameters of the related weakly nonlinear equation. To characterise such systems in general, we analysed the effects of spatio-temporal variations in the parameters of the dimensionless equation (see Supplemental Material)

$$\omega \frac{\partial A}{\partial t} = D \frac{\partial^2 A}{\partial x^2} + a + k(x,t)A - \varepsilon A^n. \tag{1}$$

In Eq. (1), $A(x,t)$ is a measure of the morphogen concentration (in terms of the deviation from the non-patterned state for the mode excited over the bifurcation [47]). The parameter $D > 0$ represents a strength of diffusion. The parameter $a \geq 0$ represents a measure of base production in terms of the excited mode; a typically vanishes for noiseless Turing systems ($n = 3$). The imposed function $k(x,t)$ represents the net strength of self-activation in comparison to decay. The parameter $\omega > 0$ represents a measure of the frequency of k variation and $\varepsilon > 0$ represents the strength of nonlinear saturation effects. The exponent $n = 2$ or 3, corresponding to the canonical weakly nonlinear form of an imperfect transcritical or a (supercritical) pitchfork bifurcation, respectively. Each of these characterises a minimal gene-regulatory motif (Fig. 1a). The case with $n = 2$ ($n = 3$) can be thought of as a modified version of the Fisher-KPP (Ginzburg-Landau) equation. Generally, to obtain the significant 'on-off' type effects seen in biological signalling, the system must be weakly nonlinear i.e. $\varepsilon \ll 1$. For ease of exposition, it is also convenient to impose $\omega \ll 1$ and $D \ll 1$. At this point, we make no fur-

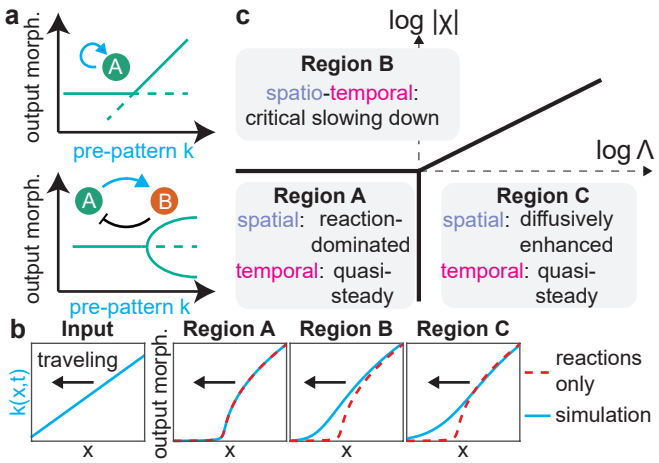

FIG. 1: General asymptotic framework for classifying dynamics of pattern-forming systems. a) Bifurcation diagrams and related minimal gene-regulatory network motifs for two classes of pattern-forming system. Top: autoinduction loops are associated with transcritical bifurcations. Bottom: activator-inhibitor systems are associated with pitchfork bifurcations. b) Examples of predicted dynamics in three different regions of parameter space (see panel c) for a travelling gradient (Eq. 2), which is a linearized form of a more general spatio-temporal variation. Results were generated by solving Eq. (1) numerically, with $n = 3$ and $k(x,t)$ specified via Eq. (2); results are similar for $n = 2$. The dashed line shows reaction-dominated results obtained by solving the steady form of Eq. (1) for each x without diffusion. c) General parameter space that classifies the system dynamics in each region for a spatio-temporal variation of the form Eq. (2). The boundary between Regions B and C occurs when $\Lambda^{2/3}/|\chi| = O(1)$ and $\Lambda, |\chi| \gg 1$.

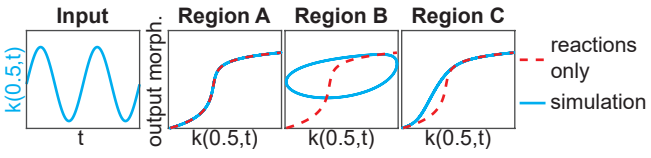

FIG. 2: Examples of predicted dynamics for a spatio-temporal oscillation in $k(x,t)$ of the form Eq. (S70), shown at a fixed x (left). Results were generated as in Fig. 1b and plotted at $x = 0.5$ in a domain of size $x = 1$ (right; y axis log scale). In Region B, the system becomes locked in the patterned state despite large oscillations in $k(x,t)$.

ther assumptions on the relative sizes of ε, ω, and D; our general results will allow us to understand the significant change in system behaviour as the relative sizes of these parameters vary. Then, in the spatio-temporally uniform system, $k < 0$ represents the unpatterned region and $k > 0$ the patterned region, with $k = 0$ defining the position of the bifurcation in homogeneous conditions.

As a simple form of spatio-temporal parameter variation, we considered the parameter $k(x,t)$ in Eq. (1) to take the form of a travelling gradient

$$k(x,t) = (x - s(t))\eta(t), \tag{2}$$

which can travel into the patterned region ($\dot{s}\eta > 0$) or into the unpatterned region ($\dot{s}\eta < 0$). This can be considered a linearized form of arbitrary spatio-temporal variations in the vicinity of a bifurcation, where we assume that η never crosses zero to avoid degeneracy. We then transformed into the frame around the moving point $x = s(t)$, at which $k = 0$. With the appropriate scaled quantities $C = (\varepsilon/a)^{1/n}A$ and $Z = (\eta/(a^{n-1}\varepsilon)^{1/n})(x-s)$, this yielded the leading-order governing equation (Supplemental Material):

$$0 = \underbrace{\Lambda(t)\frac{\partial^2 C}{\partial Z^2}}_{\text{(i)}} + \underbrace{\chi(t)\frac{\partial C}{\partial Z}}_{\text{(ii)}} + \underbrace{1}_{\text{(iii)}} + \underbrace{ZC}_{\text{(iv)}} - \underbrace{C^n}_{\text{(v)}}, \tag{3}$$

where

$$\Lambda(t) := \frac{\eta^2 D}{(a^{n-1}\varepsilon)^{3/n}}, \quad \chi(t) := \frac{\eta\omega\dot{s}}{(a^{n-1}\varepsilon)^{2/n}}. \tag{4}$$

Broadly, Λ quantifies the importance of diffusion and χ quantifies the importance of spatio-temporal changes in the parameters, both in comparison to base production. Eq. (3) can be reduced further in systems with $a = 0$ in Eq. (1), which exhibit a perfect (as opposed to imperfect) bifurcation (Supplemental Material).

We analysed Eq. (3) to characterise all possible dynamical regimes and their dependence on Λ and χ. While the quantitative results differ depending on the type of bifurcation and the direction of the travelling gradient in Eq. (2) (see Supplemental Material), we found that the qualitative behaviours split into three regions in parameter space (Fig. 1c), with key differences in the dynamical position of the bifurcation Z^* (the position at which $C = 1$ in Eq. 3):

Region A. Reaction-dominated and quasi-steady patterning. In this case, $\Lambda \ll 1$ and $|\chi| \ll 1$, and the reaction terms (iii)-(v) dominate in Eq. (3). The dynamical position of the bifurcation corresponds to its quasi-steady position, i.e. $Z^* = 0$ (Fig. 1b,c).

Region B. Critical slowing down. In this case $|\chi| \gg 1$ and $\Lambda^{2/3}/|\chi| \ll 1$, and terms (ii)-(v) dominate in Eq. (3) – saturation, i.e. term (v), can be ignored in the unpatterned part of the domain, and base production, i.e. term (iii), can be ignored in the patterned part. The dynamical position of the bifurcation lags behind its quasi-steady position, and scales as $|Z^*| = O(\sqrt{|\chi|\log|\chi|})$ (Fig. 1b,c).

Region C. Diffusively enhanced, quasi-steady patterning. In this case $\Lambda \gg 1$ and $\Lambda^{2/3}/|\chi| \gg 1$, and terms (i), (iii)-(v) dominate in Eq. (3) – saturation can be ignored in the unpatterned part of the domain, and base production can be ignored in the patterned part. The dynamical position of the bifurcation is shifted via

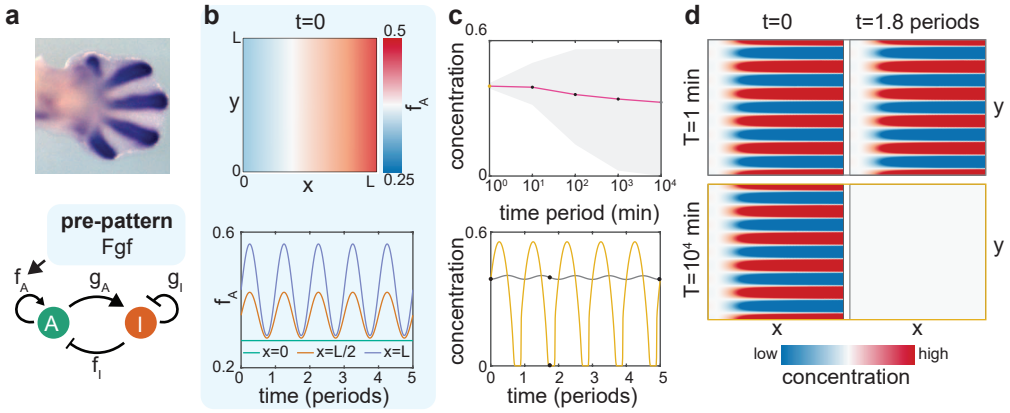

FIG. 3: Effect of spatio-temporal morphogen variations on Turing patterns. a) We model Turing patterns during digit formation (top; reproduced from [14] with permission). The system's pattern can be represented as an activator-inhibitor system, with the self-activation parameter f_A modulated by a morphogen called Fgf (bottom). b) The parameter f_A (min^{-1}) at $t = 0$ (top) and throughout the spatio-temporal oscillations Eq. (11) (bottom; Movie S1). c) Top: Effect of time period T of spatio-temporal oscillations in Fgf on the mean concentration of the activator morphogen (line), and the range of concentration (grey area) during the oscillations. Bottom: Oscillations in the activator morphogen concentration for fast ($T = 1$ min) and slow ($T = 10^4$ min) oscillations in Fgf (Movie S1). d) For oscillations that are filtered out, patterning remains the same (top). For oscillations that are not filtered out, patterning completely disappears (bottom). Images correspond to the black dots in panel c. Concentrations in the figure are non-dimensional and represent deviation from a base state at $x = 0$ [16].

diffusion towards the unpatterned part of the domain, and scales as $|Z^*| = O((\Lambda \log^2 \Lambda)^{1/3})$ (Fig. 1b,c).

These results suggest that the emergent dynamics of pattern-forming systems are determined in time and space by the regime in which the parameters lie (Fig. 1b-c). Furthermore, the results quantify how the location of a dynamic bifurcation is determined in each regime - either purely by a balance between the reaction terms for Region A, or otherwise for Regions B and C (Fig. 1b,c). In Regions B and C, diffusion and temporal variations in the parameters promote shifts in the location of the bifurcation that require an asymptotic analysis to quantify (see Supplemental Material).

Analysis for oscillatory parameters. A striking example of a shift in the bifurcation caused by temporal parameter variations is the "critical slowing down" regime, Region B, in which dynamics are slowed by passage through the bifurcation [29, 30]. We wondered whether this critical slowing down could cause a pattern-forming system to ignore the presence of a bifurcation for certain oscillatory parameter variations, even if a local balance between reaction terms would predict repeated cycles of bifurcation onset and offset. Therefore, we performed an analysis of the effect of such oscillatory variations in the system Eq. (1) (Fig. 2; Supplemental Material). We found that there is an effective inertia associated with oscillating over the bifurcation, and so each system may indeed become stuck in the unpatterned or patterned state (Fig. 2) for parameters oscillating quickly enough, even at large amplitudes. This demonstrates that the bifurcations in each system can act as low-pass filters on parameter variations (see also Fig. S1). Taken together, these analytical results suggest that pattern-forming systems with spatio-temporally varying parameters exhibit universal dynamics that are determined by the underlying bifurcations in their governing equations.

Biological systems: Models. We explored the implications of our analytical results to two paradigmatic biological pattern-forming systems with variations in pre-pattern morphogens, which affect parameters in the system gene-regulatory network [7]. The first system we considered is a model for digit formation via activator-inhibitor Turing patterns [14], in which the pre-pattern morphogen is fibroblast growth factor (Fgf), which affects the self-activation of the activator (Fig. 3a). The system is associated with a pitchfork bifurcation, and is described by the equations

$$\frac{\partial A}{\partial t} = \nabla \cdot (D_A \nabla A) + f_A(x,t)A - f_I I - f_c A^3, \qquad (5)$$

$$\frac{\partial I}{\partial t} = \nabla \cdot (D_I \nabla I) + g_A A - g_I I, \qquad (6)$$

where A and I are the concentrations of the activator and inhibitor, respectively, D_A and D_I are diffusion coefficients, and f_A, f_I, g_A, g_I and f_c are kinetic parameters (Fig. 3a, Supplemental Material). To simulate variations in Fgf [14], we let $f_A(x,t)$ vary in space and time:

$$f_A(x,t) = f_A^b + k_A f(x,t), \qquad (7)$$

where f_A^b is the base self-activation of the activator, k_A is a typical increase in the self-activation, and $f(x,t)$ is a non-dimensional concentration of Fgf.

The second system we considered is bacterial quorum sensing (QS) in *Vibrio fischeri*, which causes bioluminescence in the Hawaiian bobtail squid [31]. An autoinducer

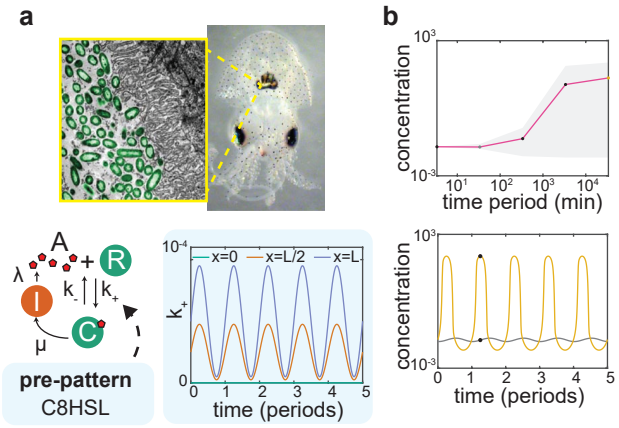

FIG. 4: Effect of spatio-temporal morphogen variations on bacterial quorum sensing in a small biofilm or cell population. a) We model quorum sensing in *V. fischeri*, which causes bioluminescence in the Hawaiian bobtail squid (top; images adapted from [28], with permission). We model the LuxR system, in which an autoinducer, 3OC6HSL, promotes its own synthesis by binding with a protein, LuxR, to form a transcription factor (bottom left). The binding parameter k_+ is modulated by competitive binding with a second autoinducer, C8HSL. Bottom right: the parameter k_+ ($\mathrm{nM}^{-1}\mathrm{s}^{-1}$) throughout the spatio-temporal oscillations Eq. (11) (see also Movie S2). b) Top: Effect of the time period T of the spatio-temporal oscillations in C8HSL on the mean 3OC6HSL concentration (line), and the range of 3OC6HSL concentration (grey area) during the oscillations. Bottom: Oscillations in 3OC6HSL concentration, for fast ($T \approx 30$ min) and slow ($T \approx 3 \cdot 10^4$ min) oscillations in C8HSL. For oscillations that are filtered out, the system remains at low 3OC6HSL concentration. For oscillations that are not filtered out, the cell population fills with 3OC6HSL during the oscillation (see Movie S2). Concentrations in the figure are scaled by the quorum sensing activation threshold of 5 nM [11].

self-activates its own expression via the canonical LuxR network; the pre-pattern morphogen is a cross-talking autoinducer [32], which interferes with self-activation of the LuxR-associated autoinducer (Fig. 4a). The system is associated with a transcritical bifurcation, and is described by the equations

$$\frac{\partial A}{\partial t} = \nabla \cdot (D \nabla A) + \rho f_A(A, I, R, C; x, t) - \kappa A, \tag{8}$$

$$\frac{\partial I}{\partial t} = f_I(I, C), \; \frac{\partial R}{\partial t} = f_R(A, R, C), \; \frac{\partial C}{\partial t} = f_C(A, R, C). \tag{9}$$

where, D is the diffusivity of the autoinducer, ρ is the cell volume fraction, κ is the autoinducer decay rate, and the reaction terms inside each bacterium, including the effect of cross-talk, are defined by the gene-regulatory network (Fig. 4a, Supplemental Material).

In each system, we considered two types of spatio-temporal variation in the pre-pattern morphogen $f(x,t)$. For analysis, we used a linear gradient in space travelling with constant speed,

$$f(x,t) = x/L - t/T, \tag{10}$$

to relate the system dynamics to the analytical results in Fig. 1. In simulations, performed in the finite-element computational software COMSOL Multiphysics in 2D, we used a linear gradient in space and a sinusoidal oscillation in time

$$f(x,t) = (x/L)\,(1 + K \sin(2\pi t/T))\,, \tag{11}$$

to investigate numerically the robustness of each system to spatio-temporal fluctuations (see Movies S1 and S2). In Eq. (10) and Eq. (11), T quantifies the timescale of variation, and K in Eq. (11) quantifies the relative magnitude of the oscillation.

Biological Systems: Analytical Results. By analysing each system, we found that with pre-pattern morphogen variations of the form Eq. (10), each model reduces to the appropriate version of Eq. (3), and $\Lambda(t)$ and $\chi(t)$ written in terms of the kinetic parameters (Eqs. S36 and S74). Therefore, both of the paradigmatic pattern-forming systems considered here are subject to the universal regimes we have identified, a consequence of their bifurcation structures. We therefore used our analytical results to predict the effect of physiological spatio-temporal variations in pre-pattern morphogens in each system. We chose physiologically relevant values of the parameters in both systems (Tables S1, S2), with the timescale of variation T in Eq. (10) corresponding to the relevant growth timescale, in line with experimental evidence that suggests physiological changes to patterning in each system are induced by growth [14, 16, 33]. Our analysis predicts that for such parameters, each system sits in Regime C of parameter space (diffusively enhanced patterning; see Fig. 1c), with significant quantitative differences between the two systems. In the Turing system, the diffusive enhancement to patterning is less than 10% of the domain (Table S1) – patterning would be expected to be controlled relatively locally by the concentration of the pre-pattern morphogen Fgf. This prediction is in line with recent analyses of Turing systems in steady pre-pattern morphogen gradients, in which patterning was found to be controlled relatively locally in space [10]. By contrast, our analysis predicts that diffusive enhancement to patterning is much stronger in the bacterial quorum sensing system. We found that diffusive enhancement causes the patterned (or QS-activated) region to be larger than the size of the population (Table S2) – any local activation in QS caused by changes over a growth timescale would be expected to cause the entire population to activate. This would benefit the population by ensuring all cells commit together to a multicellular program of gene expression, as was recently found in fluid flows [11]. These results demonstrate that biological pattern-forming systems can tune via diffusion the extent of patterning.

Biological Systems: Numerical Results. Interestingly, by varying the timescale T in Eq. (10), in each system we found that if pre-pattern morphogen changes occur fast enough, the system transitions to Region B (critical slowing down) of parameter space. This suggested exploring the biological relevance of our analytical prediction of low-pass filtering for fast oscillatory morphogen variations. To this end, we simulated oscillations of the form Eq. (11) in each system (Fig. 3b; Fig. 4b). In agreement with our analysis, we found a critical oscillation timescale, which we calculated to be around 3-10 hours, depending on the kinetic parameters in each system (Fig. 3c; Fig. 4c; Fig. S1) – surprisingly, this is a few hours faster than the timescale of growth in both systems (Tables S1, S2). Our simulations confirmed that, for oscillations over faster timescales, morphogen variations occur fast enough to cause the system to remain stuck in the unpatterned or patterned state, because of the critical slowing down in the system (Fig. 3c,d; Fig. 4c,d). Therefore, we expect changes in the pre-pattern morphogen concentration to be ignored if they occur much faster than a growth timescale, allowing the system to avoid repeated cycles of complete removal of patterning (Fig. 3d, Fig. 4d). Remarkably, this suggests that the gene-regulatory parameters in each biological system are tuned such that each system is robust to non-physiological variations in pre-pattern morphogens.

Discussion and Conclusion. In modelling these biological systems we have performed significant simplifications for clarity and generality. In particular, we have not modelled the effect of white noise, which we expect to have effects that are not captured by our analysis [34, 35]. Furthermore, our models are effective macroscopic representations of microscopic processes, and the process of coarse-graining the microscopic dynamics to obtain effective macroscopic dynamics is often not trivial [36].

To conclude, we have presented a general framework that classifies and quantifies the dynamic response of pattern-forming systems to spatio-temporal variations in their parameters. The framework complements recent work on pattern formation in various systems of equations with spatio-temporally varying parameters (e.g. [10, 37–44]). We have applied our framework to simple models of two biological pattern-forming systems, each with variations in a pre-pattern morphogen that affects kinetic parameters: digit formation via Turing patterns, and bacterial quorum sensing. Our theory predicts that both systems filter out spatio-temporal morphogen variations that occur much faster than growth. We demonstrate that the type of bifurcation in the system, which is determined by the gene-regulatory network, controls emergent patterning dynamics and structure. Predictions such as these are testable in newly developed systems that allow spatio-temporal control over gene-expression and the external environment, such as synthetic model organisms [45], organoids [46] and microfluidic devices [23]. Owing to the generality of the canonical equations that we have analysed, our theoretical framework is extendable to a wide class of pattern-forming systems.

Acknowledgments. MPD is supported by the UK Engineering and Physical Sciences Research Council [Grant No. EP/W032317/1]. PP is supported by a UKRI Future Leaders Fellowship [MR/V022385/1]. We thank Zena Hadjivasiliou and Jake Cornwall Scoones for helpful discussions, and Eric Stabb for assistance with Fig. 4a.

* m.dalwadi@ucl.ac.uk; equal contribution
† philip.pearce@ucl.ac.uk; equal contribution

[1] Alon, U. *An Introduction to Systems Biology* (Chapman and Hall/CRC, Second edition. — Boca Raton, Fla. : CRC Press, [2019], 2019).
[2] Vittadello, S. T., Leyshon, T., Schnoerr, D. & Stumpf, M. P. H. Turing pattern design principles and their robustness. *Philosophical Transactions of the Royal Society A: Mathematical, Physical and Engineering Sciences* **379** (2021).
[3] Eldar, A. *et al.* Robustness of the BMP morphogen gradient in Drosophila embryonic patterning. *Nature* **419**, 304–308 (2002).
[4] Wartlick, O. *et al.* Dynamics of Dpp Signaling and Proliferation Control. *Science* **331**, 1154–1159 (2011).
[5] Mateus, R. *et al.* BMP Signaling Gradient Scaling in the Zebrafish Pectoral Fin. *Cell Reports* **30**, 4292–4302 (2020).
[6] Scholes, N. S., Schnoerr, D., Isalan, M. & Stumpf, M. P. A Comprehensive Network Atlas Reveals That Turing Patterns Are Common but Not Robust. *Cell Systems* **9**, 243–257 (2019).
[7] Green, J. B. A. & Sharpe, J. Positional information and reaction-diffusion: two big ideas in developmental biology combine. *Development* **142**, 1203–1211 (2015).
[8] Jutras-Dubé, L., El-Sherif, E. & François, P. Geometric models for robust encoding of dynamical information into embryonic patterns. *eLife* **9**, 1–36 (2020).
[9] Cornwall Scoones, J. & Hiscock, T. W. A dot-stripe Turing model of joint patterning in the tetrapod limb. *Development* **147** (2020).
[10] Krause, A. L., Klika, V., Woolley, T. E. & Gaffney, E. A. From one pattern into another: Analysis of Turing patterns in heterogeneous domains via WKBJ. *Journal of the Royal Society Interface* **17** (2020).
[11] Dalwadi, M. P. & Pearce, P. Emergent robustness of bacterial quorum sensing in fluid flow. *Proceedings of the National Academy of Sciences of the United States of America* **118**, e2022312118 (2021).
[12] Krause, A. L., Gaffney, E. A., Maini, P. K. & Klika, V. Modern perspectives on near-equilibrium analysis of Turing systems. *Philosophical Transactions of the Royal Society A: Mathematical, Physical and Engineering Sciences* **379** (2021).
[13] Turing, A. M. The chemical basis of morphogenesis. *Philosophical Transactions of the Royal Society of London. Series B, Biological Sciences* **237**, 37–72 (1952).
[14] Sheth, R. *et al.* Hox Genes Regulate Digit Patterning by Controlling the Wavelength of a Turing-Type Mecha-

nism. *Science* **338**, 1476–1480 (2012).

[15] Paulsson, J. Summing up the noise in gene networks. *Nature* **427**, 415–418 (2004).

[16] Raspopovic, J., Marcon, L., Russo, L. & Sharpe, J. Digit patterning is controlled by a Bmp-Sox9-Wnt Turing network modulated by morphogen gradients. *Science* **345**, 566–570 (2014).

[17] Ward, J. P. *et al.* Early development and quorum sensing in bacterial biofilms. *Journal of Mathematical Biology* **47**, 23–55 (2003).

[18] Daniels, R., Vanderleyden, J. & Michiels, J. Quorum sensing and swarming migration in bacteria. *FEMS Microbiology Reviews* **28**, 261–289 (2004).

[19] Bhattacharyya, S. & Yeomans, J. M. Coupling Turing stripes to active flows. *Soft Matter* **17**, 10716–10722 (2021).

[20] Fulton, T. *et al.* Cell Rearrangement Generates Pattern Emergence as a Function of Temporal Morphogen Exposure. *bioRxiv* (2022).

[21] Wigbers, M. C. *et al.* A hierarchy of protein patterns robustly decodes cell shape information. *Nature Physics* **17**, 578–584 (2021).

[22] Patel, K., Rodriguez, C., Stabb, E. V. & Hagen, S. J. Spatially propagating activation of quorum sensing in Vibrio fischeri and the transition to low population density. *Physical Review E* **101**, 062421 (2020).

[23] Kim, M. K., Ingremeau, F., Zhao, A., Bassler, B. L. & Stone, H. A. Local and global consequences of flow on bacterial quorum sensing. *Nature Microbiology* **1**, 15005 (2016).

[24] Mukherjee, S. & Bassler, B. L. Bacterial quorum sensing in complex and dynamically changing environments. *Nature Reviews Microbiology* **17**, 371–382 (2019).

[25] Pearce, P. *et al.* Flow-Induced Symmetry Breaking in Growing Bacterial Biofilms. *Physical Review Letters* **123**, 258101 (2019).

[26] Brauns, F., Halatek, J. & Frey, E. Phase-Space Geometry of Mass-Conserving Reaction-Diffusion Dynamics. *Physical Review X* **10**, 041036 (2020).

[27] Strogatz, S. H. *Nonlinear Dynamics and Chaos* (CRC Press, 2015).

[28] Stabb, E. V. The Vibrio fischeri - Euprymna scolopes Light Organ Symbiosis. In *The Biology of Vibrios*, 204–218 (ASM Press, Washington, DC, USA, 2014).

[29] Gomez, M., Moulton, D. E. & Vella, D. Critical slowing down in purely elastic 'snap-through' instabilities. *Nature Physics* **13**, 142–145 (2017).

[30] Liu, M., Gomez, M. & Vella, D. Delayed bifurcation in elastic snap-through instabilities. *Journal of the Mechanics and Physics of Solids* **151**, 104386 (2021).

[31] Visick, K. L., Stabb, E. V. & Ruby, E. G. A lasting symbiosis: how Vibrio fischeri finds a squid partner and persists within its natural host. *Nature Reviews Microbiology* **19**, 654–665 (2021).

[32] Pérez, P. D., Weiss, J. T. & Hagen, S. J. Noise and crosstalk in two quorum-sensing inputs of Vibrio fischeri. *BMC Systems Biology* **5**, 153 (2011).

[33] Singh, P. K. *et al.* Vibrio cholerae Combines Individual and Collective Sensing to Trigger Biofilm Dispersal. *Current Biology* **27**, 3359–3366 (2017).

[34] Coomer, M. A., Ham, L. & Stumpf, M. P. Noise distorts the epigenetic landscape and shapes cell-fate decisions. *Cell Systems* **13**, 83–102 (2021).

[35] Karig, D. *et al.* Stochastic Turing patterns in a synthetic bacterial population. *Proceedings of the National Academy of Sciences* **115**, 6572–6577 (2018).

[36] Michailidi, M. R. *et al.* Morphogen gradient scaling by recycling of intracellular Dpp. *Nature* (2021).

[37] Page, K., Maini, P. K. & Monk, N. A. Pattern formation in spatially heterogeneous Turing reaction-diffusion models. *Physica D: Nonlinear Phenomena* **181**, 80–101 (2003).

[38] Page, K. M., Maini, P. K. & Monk, N. A. Complex pattern formation in reaction–diffusion systems with spatially varying parameters. *Physica D: Nonlinear Phenomena* **202**, 95–115 (2005).

[39] Cuesta, C. M. & King, J. R. Front propagation in a heterogeneous fisher equation: The homogeneous case is non-generic. *Quarterly Journal of Mechanics and Applied Mathematics* **63**, 521–571 (2010).

[40] Woolley, T. E., Krause, A. L. & Gaffney, E. A. Bespoke Turing Systems. *Bulletin of Mathematical Biology* **83**, 41 (2021).

[41] Goh, R. & Scheel, A. Pattern-forming fronts in a Swift–Hohenberg equation with directional quenching — parallel and oblique stripes. *Journal of the London Mathematical Society* **98**, 104–128 (2018).

[42] Rüdiger, S., Nicola, E. M., Casademunt, J. & Kramer, L. Theory of pattern forming systems under traveling-wave forcing. *Physics Reports* **447**, 73–111 (2007).

[43] Liu, Y., Maini, P. K. & Baker, R. E. Control of diffusion-driven pattern formation behind a wave of competency. *arXiv* (2021).

[44] Würthner, L. *et al.* Bridging scales in a multiscale pattern-forming system. *arXiv* (2021).

[45] di Pietro, F. *et al.* Rapid and robust optogenetic control of gene expression in Drosophila. *Developmental Cell* **56**, 3393–3404 (2021).

[46] Hofer, M. & Lutolf, M. P. Engineering organoids. *Nature Reviews Materials* **6**, 402–420 (2021).

[47] For example, for Turing bifurcations with $n = 3$, A typically represents the envelope amplitude for the patterned state, as predicted by the fastest growing mode at the onset of instability.